Chapter 11

Microscale Energy Harvesters with Nonlinearities Due to Internal Impacts

Cuong Phu Le and Einar Halvorsen

Additional information is available at the end of the chapter

http://dx.doi.org/10.5772/52048

1. Introduction

Energy harvesting from mechanical vibrations is one among several alternatives currently considered as power sources for wireless devices. The main motivation is the prospect of eliminating maintenance or increasing maintenance intervals by providing a means for recharging batteries or replacing batteries altogether. Energy harvesting can also be an enabling technology for applications where operating conditions, e.g. temperature, inhibit use of batteries. The prospect of reducing system size can also be a factor of interest. Vibration energy harvesting is therefore a topic of great interest in the scientific community [1-6], especially regarding miniaturized devices. For macro scale devices, commercial products have already emerged [7].

A vibration energy harvester is usually a spring-mass-damper system with a transducer that is continuously driven by the relative motion of the mass with respect to a device frame. The transducers are typically one of the three main types: electromagnetic, piezoelectric or electrostatic [1-2, 8-14]. For small scale systems, vibration energy harvesters face at least two fundamental obstacles. Reduced size necessarily means reduced mass, meaning reduced output power in an inertially driven device. Furthermore, the smaller harvesters have smaller space available for proof mass motion which again limits the distance over which work can be done.

In practical generators, mechanical end-stops are intentionally designed in order to confine the displacement of the inertial mass to the finite die dimension and to avoid spring fracture or degradation of material properties. When the acceleration amplitude is sufficient for proof-mass impacts on end-stops to occur, non-linear effects such as the jump phenomenon in the displacement vs. frequency response appear. Even though this behavior can be exploited to extend device bandwidth, operating a conventional harvester in this regime has the considerable disadvantage that the output power saturates at high excitation levels and

therefore the effectiveness of the device decreases. This saturation is quite generic and has been reported for a variety of devices [15-20].

This chapter is concerned with the extent to which the internal impacts on these end-stops can be exploited by making transducing end-stops. Several prototypes utilizing impact principles in macroscale piezoelectric devices have been presented [21-28]. Here we consider microscale electrostatic energy harvesters with two types of transducers, main transducer and secondary end-stop transducers. At sufficiently strong excitations, the impact of the proof-mass onto the end-stops actuates the secondary transducer and thereby harvests the excess kinetic energy of the proof mass. Therefore, the device provides power through two states as excitation strength increases, a first stage with only primary transducer output, and a second stage with output from all transducers.

For a velocity damped generator, the end-stop limit is reached when $AQ=Z_L\omega_0^2$ where A is the package acceleration, Q is the total (loaded) quality factor, ω_0 is the angular resonant frequency and Z_L is the maximum displacement. In a previous work [29], we demonstrated the concept on an open device with a relatively high mechanical Q of about 200. Here, we demonstrate the concept on an encapsulated device with a rather low Q of about 4. As in [29], we compare to a reference device of the same die dimensions.

Section 2 of this chapter details the motivation and working principle for the impact-based electrostatic device. The MEMS-implementation of the concept, made in the Tronics MPW foundry process [31], is described in detail in Section 3, modelled in Section 4 and characterized in Section 5.

2. Device principles

A schematic model of a traditional harvester is shown in Figure 1. With such a design, the typical behavior in frequency sweeps is a clipping of the resonance peak and the occurrence of a jump phenomenon on the high frequency side of the clipped peak. With increasing amplitude, the output power eventually saturates, at least approximately. These effects have been observed in several devices, e.g. in a mesoscale electromagnetic harvester by [16], a mesoscale piezoelectric harvester [18-19] and a microscale electrostatic harvester [17]. Some examples of measured and simulated characteristics of a microscale electrostatic energy harvester from [30] are shown in Figure 2 which displays “clipping“ of the response and extended up-sweep bandwidth, and Figure 3 which displays saturation.

The clipping of the response in Figure 2 and the saturation in Figure 3 are direct negative consequences of the displacement limit. Whether the end-stop impacts are elastic or give loss of kinetic energy, is not significant for the output power when the vibrations are sinusoidal and at the resonant frequency [19]. Loss at end-stop impacts mainly affects the phase relationship between the driving force and the displacement. This has consequences for the value of the jump-down frequency in the up-sweep (at about 1450 Hz in Figure 2) and the details of displacement waveform. The displacement waveform may even show period doubling or chaotic-like behaviour without significant deviation from the saturation

characteristic in Figure 3, see [32]. If we are mainly concerned with vibrations at the resonant frequency, we are then free to design the end-stop with any degree of loss that we deem suitable without compromising the output power performance.

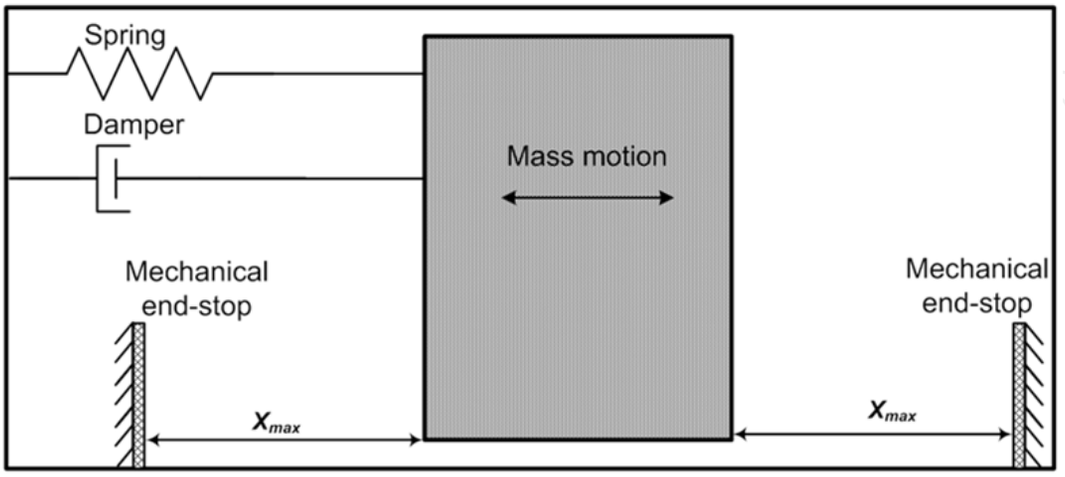

Figure 1. A schematic illustration of typical energy harvesters including a spring-dashpot mass system with use of mechanical end-stops to limit mass motion

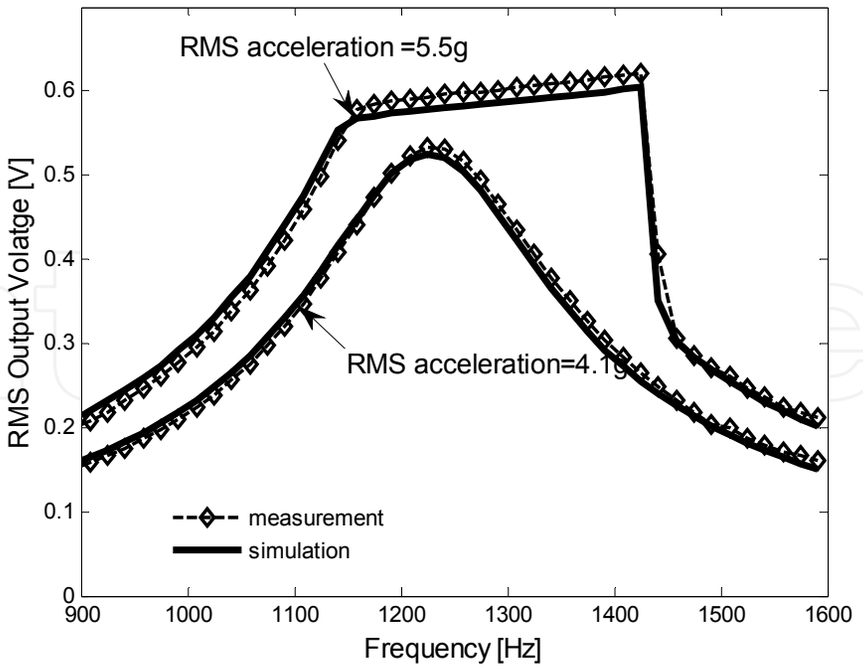

Figure 2. Up-sweep frequency response of RMS output voltage for different acceleration levels at bias voltage V_b=30V. From [30].

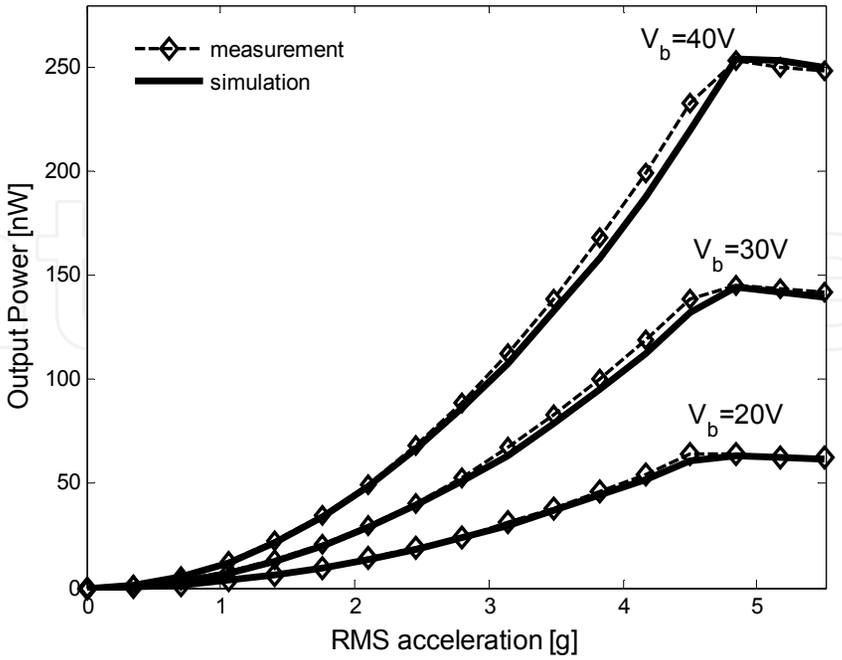

Figure 3. Output power versus acceleration amplitude for different bias voltages. From [30].

The observation that end-stop loss is not important suggests that it can be beneficial to design end-stops that are also transducers. The concept is illustrated by velocity damped end-stops in Figure 4. If these secondary transducers can scavenge significant proof-mass kinetic energy at each impact and convert it to electrical energy, we obtain power in addition to that already available from a primary transducer that will be present and associated with the proof-mass motion anyway. The questions are then how these transducing end-stops can be made and, since some chip real estate must be allocated for them, if this approach has any advantages over using the entire area for a conventional device.

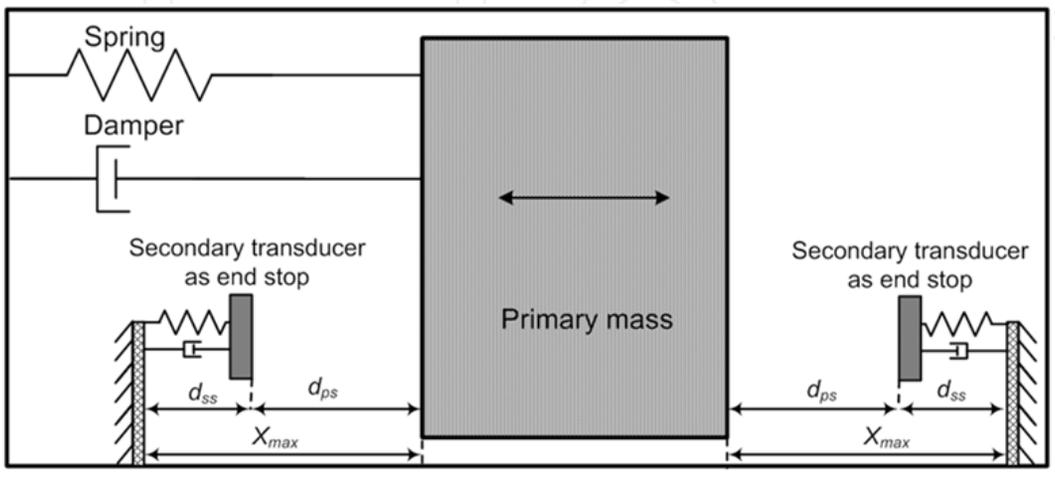

Figure 4. A schematic illustration of device concept with use of end-stops as additional transducers

3. MEMS devices

Here we consider a MEMS realisation of a device based on internal impacts as motivated in the previous section.

3.1. Impact device

Figure 5 shows an impact-device design. There are three independently suspended structures that constitute the device: one primary mass with its electrostatic transducer (ET1) and two secondary electrostatic structures with their own transducers (ET2) acting as end-stops to prevent the ET1 proof mass motion. The ET1 is an ordinary comb-drive structure driven by a movable proof mass m_{P} attached to four linear-springs with total stiffness k_{P} and a corresponding damping coefficient b_{P}. For in-plane motion of the primary mass, the output power is scavenged by the ET1 transducer which has two overlap-varying capacitances with opposite phase. The ET1 transducer is characterised by a capacitor finger length l_{P}, a capacitor finger width w_{P}, gap between fingers g_{P}, an nominal finger overlap $x_{0\mathrm{P}}$ and N_{P} fingers on each side.

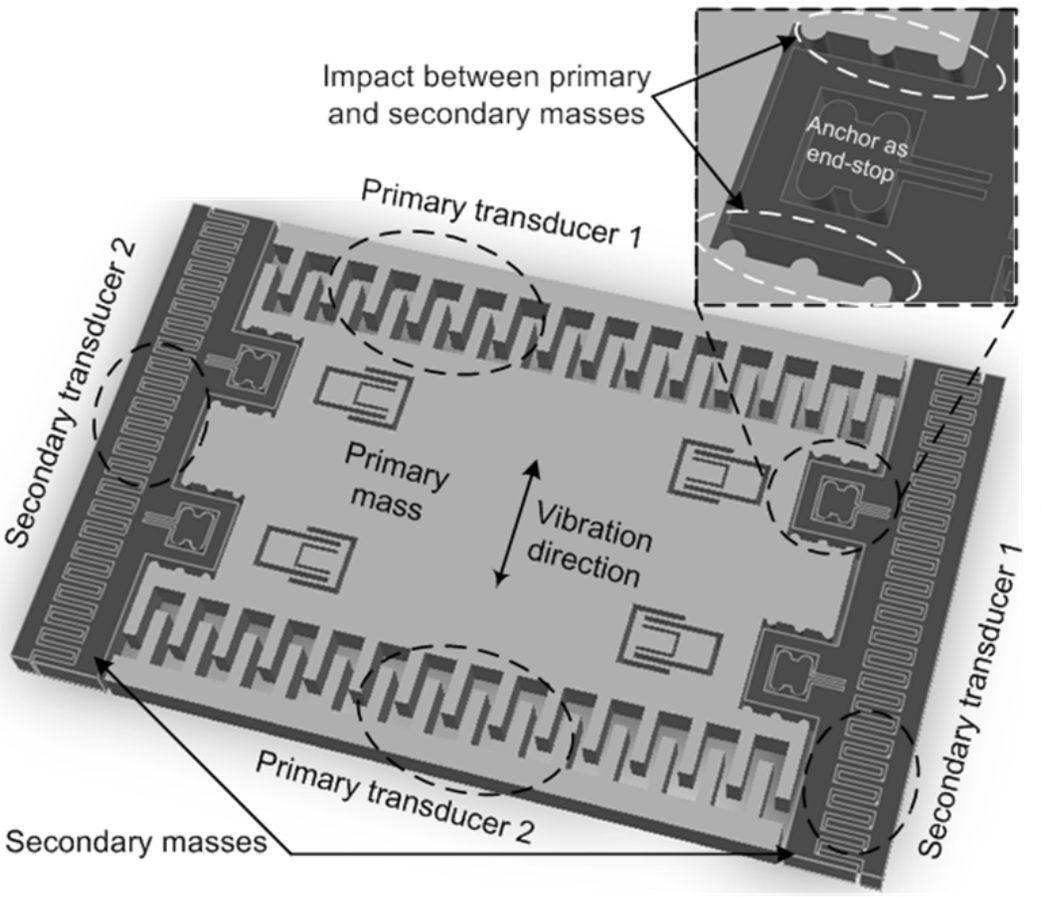

Figure 5. Schematic layout of the impact device with additional secondary electrostatic transducers functioning as end-stops for the primary mass

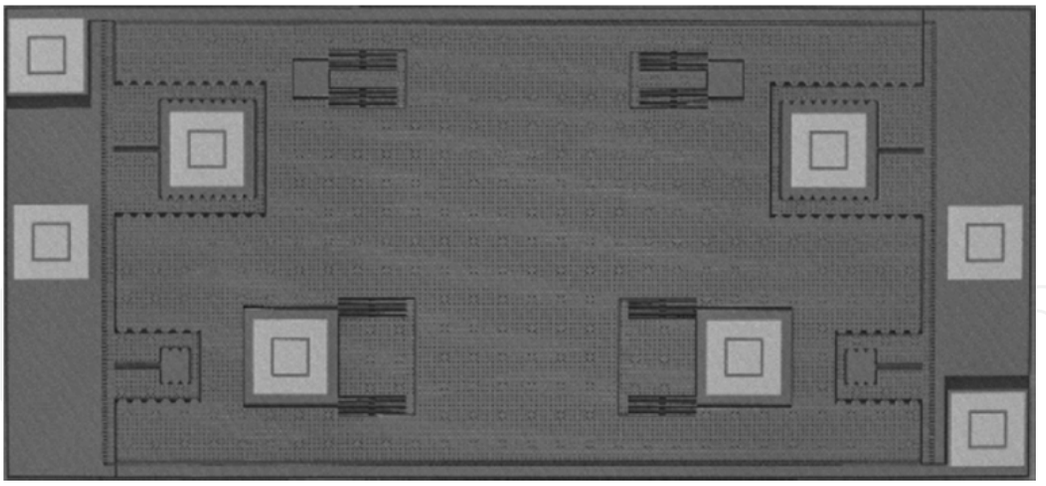

Figure 6. A total view of the impact device with primary and secondary electrostatic transducers (Photograph: Tronics Microsystems S.A.)

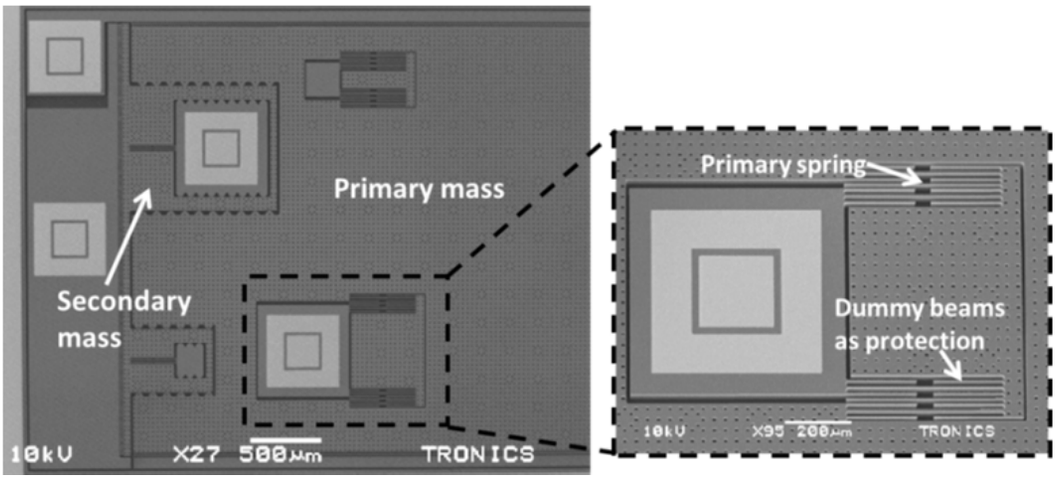

Figure 7. A close-up view of the primary and secondary transducers of the impact device (Photograph: Tronics Microsystems S.A.)

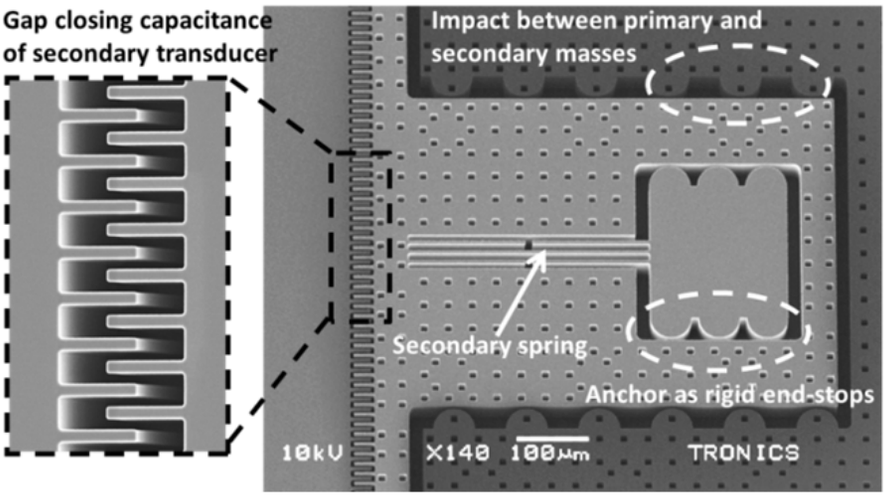

Figure 8. Secondary spring and gap-closing transducer of the secondary structure (Photograph: Tronics Microsystems S.A.)

The ET2 transducer has a mass m_s and a mechanical damping b_s. The ET2 suspension is designed as two single beams with a total spring stiffness of k_s, giving much larger resonant frequency than that of the ET1. The ET2 uses a gap varying capacitance with capacitor finger length l_s, finger width w_s, finger overlap x_{0s} and a nominal capacitor gap g_s. The number of fingers is N_s for each ET2 electrode. Rigid end-stops are used to limit the ET2 motion under overload conditions. The gap varying transducer was chosen for ET2 in order to obtain a large capacitance variation for a small displacement.

The ET1 and ET2 are accelerated in the same direction. Assuming negligible inertial actuation of the secondary structure, the impact between the primary and secondary masses occurs when the displacement amplitude of the primary mass reaches the limit d_{ps}, exciting the secondary transducers to generate extra output power. The maximum displacement amplitude of the secondary mass is d_{ss}. The impact is a contact of bumps on flat surface designed on the mass shape. The cylindrical bumps have semi-cylindrical geometry with radius R. The modelling of this kind of structures was investigated in [30].

The die is 8×4mm^2 and is fabricated in the Tronics MPW (multi-project wafer) service with high aspect ratio micromachining of the 60μm thick device layer of Silicon-on-Insulator (SOI) wafers [31]. Figure 6 shows the full view of the device. The ET2 mass m_s is significantly smaller than the ET1 mass m_p, m_p=14m_s. Effort is made to utilize the available area. Placing the supports within the area of the proof mass, makes sure a minimum area is wasted so the proof mass can be as large as possible while leaving the entire length of proof mass available for the comb-drives.

Figure 7 shows a close-up view of the primary and secondary masses. The ET1 proof mass is attached to four springs. The springs in this device are designed as folded flexures with released stress in the axial direction, resulting in the linear beams for transverse motion. The ET2 spring design makes use of two single beams separated by a distance of 2.5mm, giving linear behavior within the ET2-structure travel length. In order to secure predictable beam widths, protection beams oriented in parallel with the spring beams are included to reduce over-etching of the spring beam during fabrication. With this counter measure, we expect the beam cross-section to be closer to the ideal rectangular shape, and therefore its stiffness to be close to the design value. The measured resonance frequency deviates approximately 1.5% from the design value.

There are four metal pads on anchors: two placed on the ET1's anchors and two deposited on the ET2's anchors. They connect to voltage sources used for external biasing in the experiments. Four remaining metal pads are placed on the fixed electrodes to connect the external load resistances.

Figure 8 presents details of the ET2. We see the gap-closing transducer and the bump geometry for the contact regions between the ET1 and ET2 structures. The spring anchors of the ET2 structure also function as rigid end-stops that restrict maximum displacement of both ET1 and ET2 structures to avoid contact between fixed and counter electrodes. All of the device parameters for the ET1 and the ET2 are listed in Table 1.

Parameters	Primary structure	Secondary structure
Die dimensions	$8\times4mm^2$	
Device thickness, t	60μm	
Length of capacitor fingers, l_p, l_s	25μm	30 μm
Width of capacitor fingers, w	4μm	4μm
Gap between capacitor fingers, g_p, g_s	3.0μm	3.5μm
Number of capacitor fingers on each electrode, N_p, N_s	416	225
Nominal capacitor finger overlap, x_{0p}, x_{0s}	10μm	25 μm
Length of spring	500μm	350μm
Width of spring	6.5μm	5.2μm
Distance between primary and secondary masses, d_{ps}	4.0μm	
Distance between secondary mass and rigid end stops, d_{ss}	3.0μm	
Bump radius, R	30μm	

Table 1. Parameters of the impact device: primary and secondary electrostatic transducers

3.2. Reference device

Figure 8 shows a view of the reference device with its in-plane overlap-varying transducer. The transducer is similar to the primary transducer of the impact device. Both device prototypes have the same chip dimension. The reference transducer has a larger area for the proof mass and a slightly higher transducer capacitance than the ET1. This is due to more space being available within the same chip real-estate when there are no transducing end-stops. The reference proof mass is suspended by four folded flexure beams. The beams are connected to fours anchors acting as rigid end-stops to confine maximum displacement of the proof mass. This device was described in detail in [30] where end-stop modeling was studied.

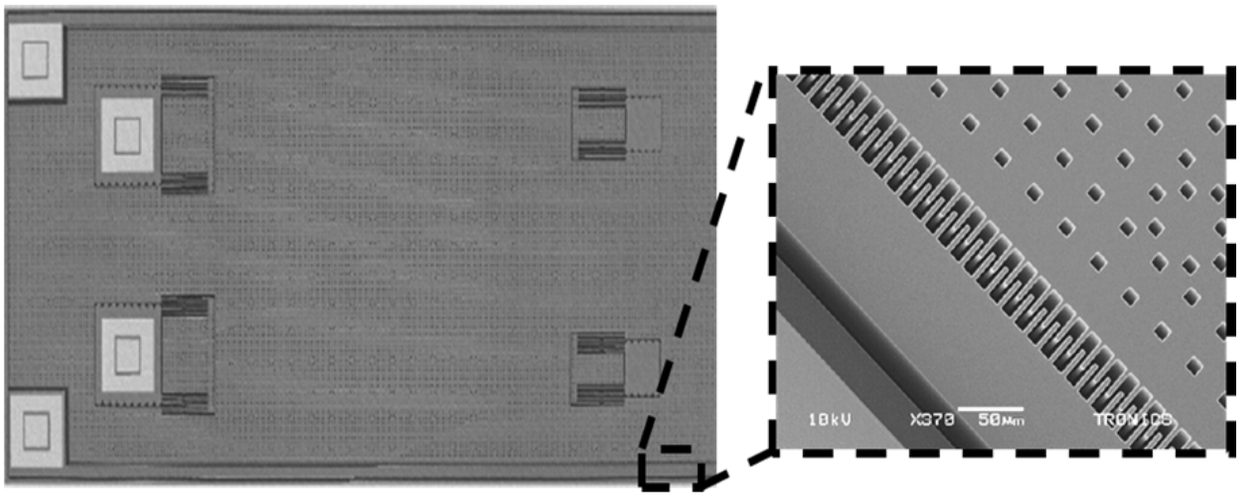

Figure 9. A view of the reference device with the same die dimension [30] (Photograph: Tronics Microsystems S.A.)

The reference transducer is also biased externally. The output voltage is simply connected to load resistance via the metal pads deposited on the fixed electrodes. Further details of the reference-device geometry can be found in [30].

4. Modelling

As a check that the device operates according to our understanding, we will compare measurements to simulation. At the lumped-model level, the device dynamics is governed by a few nonlinear differential equations that can be solved by a variety of numerical tools. We prefer to use a circuit simulator as a solver, i.e. LT-SPICE, and therefore need to formulate the dynamics as an equivalent circuit. The overall scheme of the modelling is the same as we previously used for our previous MEMS devices [30]. Special features here are that there are 3 mechanical degrees of freedom in the impact device, the proof mass position and the position of each of the two secondary structures, and that the impacts are very crucial for the operation.

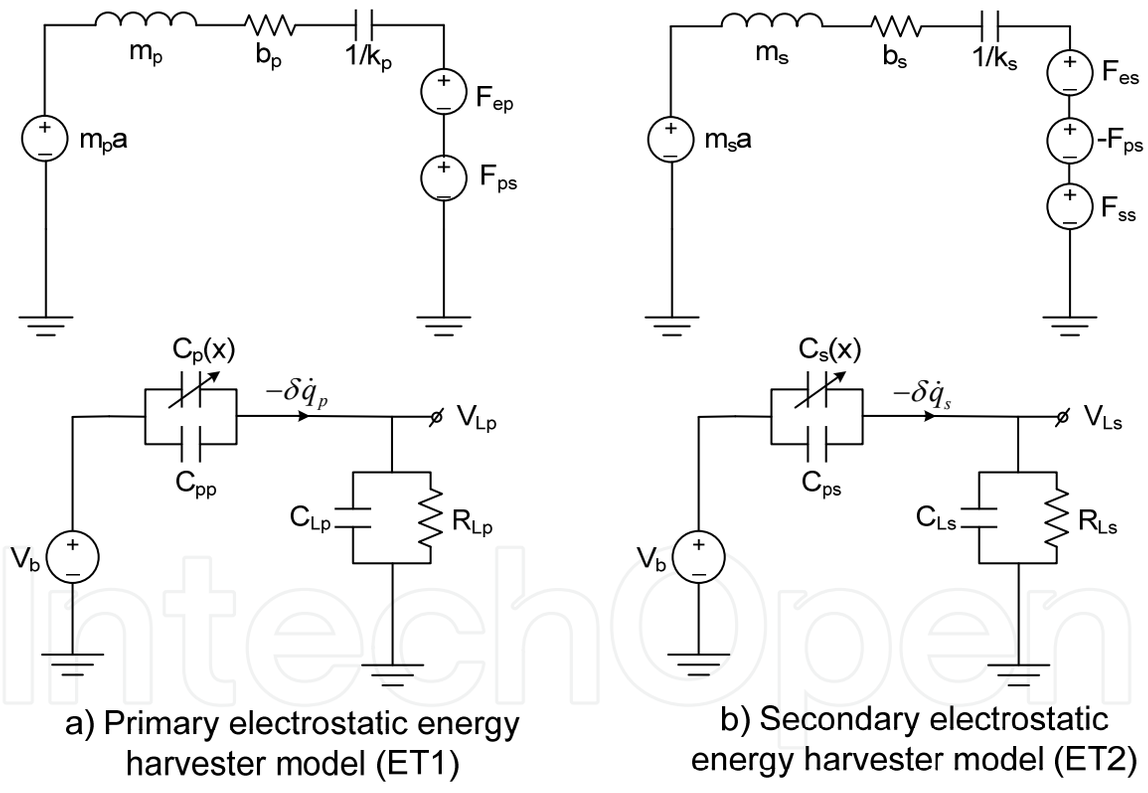

Figure 10. Lumped model of the impact device: a) primary electrostatic transducer (ET1) and b) secondary electrostatic transducer (ET2) in one port

The device is modeled as showed in Figure 10 which gives equivalent circuits for the mechanical and electrical parts of the primary structure and of a secondary structure. The proof mass displacement of the ET1 and ET2 are characterized by two variables x_p and x_s giving the displacement from the nominal position. An impact between the primary and secondary masses takes place for the relative displacement beyond the limit of d_{ps}. Similar

to the reference device, the ET2 design also has its own rigid end-stops to prevent its proof mass motion from extremely high acceleration which probably causes collapsing effects. The rigid end-stops are engaged for secondary displacements larger than a maximum distance d_{ss}. The force F_{ss} between the ET2 and the rigid end-stops are modeled using behavioral voltage sources as described in [30]. All model parameters of the impact device are listed in Table 2. Both ET1 and ET2 have the same bias voltage V_b. Due to the similar design of the reference device and the primary ET1, their optimal load resistances are almost equal. For simplicity the ET2s are also connected to the same load resistance R_L as the reference device and ET1, giving a straightforward later comparison between the outputs of the two devices.

Parameters	**Primary ET1**	**Secondary ET2**
Inertial proof mass, m_p, m_s	2.1mg	0.15mg
Spring stiffness, k_p, k_s	115.1N/m	29.5N/m
Damping coefficient, b_p, b_s	4.0e-3Ns/m	0.2e-3Ns/m
Nominal variable capacitance, C_{0p},C_{0s}	1.3pF	1.6pF
Parasitic capacitance, C_{pp}, C_{ps}	17.9pF	6.0pF
Load resistance, R_{Lp}, R_{Ls}	4.9MΩ	4.9MΩ
Load parasitic capacitance, C_{Lp}, C_{Ls}	4.2pF	2.0pF

Table 2. Model parameters of the impact device: primary and secondary electrostatic transducers

5. Measurements

Figure 11 shows the frequency response of the impact device compared with the reference device response for an RMS acceleration of 0.71g and a bias voltage V_b=7V in linear regime. At the small acceleration level, the primary mass motion is below limit and then there is no impact between the masses. The output power of the impact device is mainly from the ET1 transducers. The simulation results fit well to the measured results. The ET1 behaves similarly to the reference device. In design, the resonance frequency of the ET1 is the same as that of the reference device, but due to the over-etching effects, the ET1 resonance frequency is slightly smaller, about 1168Hz. The output power of the reference device is bigger than that of the ET1 at the same frequency. For example at the resonance frequency, the ET1 output power is 0.06nW, about three times less than the value of the reference device. The lower output power of the primary transducers originates from the smaller primary mass m_p<m and the smaller transducer capacitance C_{0p}<C_0. This is due to the area sacrificed for the secondary transducers in the impact design.

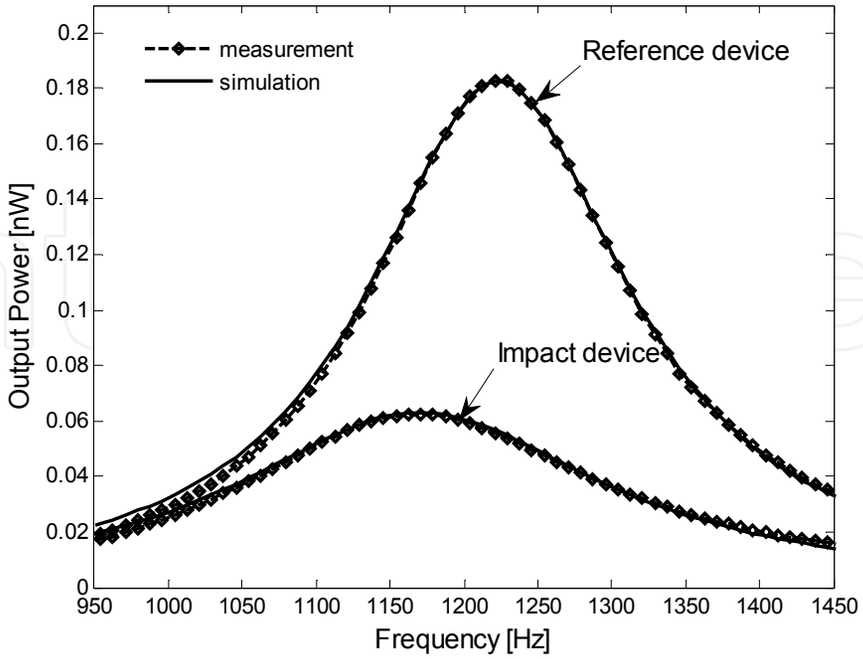

Figure 11. Frequency response of the impact device compared to the reference device for bias voltage V_b=7V and RMS acceleration of 0.71g

Fig. 12 shows the output power for frequency up-sweeps for each transducer in the reference and impact devices at A_{rms}=5.5g, which is sufficient to cause impacts between the primary and secondary masses. Compared with the reference output power, the primary output power is still smaller around the resonant frequency. The output power of the secondary transducer is significant in a frequency range from 1.15kHz to 1.30kHz. For example, at a frequency f=1.22kHz, the secondary output power is 108nW, but the output power of the reference and primary transducers is only 3.0nW and 1.4nW respectively. The energy from the impact is effectively utilized by the high transduction of the secondary transducers in the impact device. The nonlinear effect of the rigid end-stops is evident in the reference output response as saturation of the output power and occurrence of the jump phenomenon. The impacts have no performance benefit beyond up-sweep bandwidth enhancement in the reference device. Performance of the impact device is also modeled and simulated. The simulation results capture the main features of the measurements and thereby confirm that the essential mechanisms in the device have been identified.

A wider response bandwidth is obtained in simulation for the secondary transducer, while the primary transducer response behaves qualitatively like the measured result. The main differences between the measured and simulated results can be explained from the modeling of the impacts. We have seen in the simulations that when varying the loss in the impact model, the bandwidth is affected so inaccuracy in the loss representation can be at least partly responsible for the discrepancy. In addition, the design values for the device geometry have been used in the model and therefore small deviations in the distance of travel before impact could influence the impact events and thereby the bandwidth.

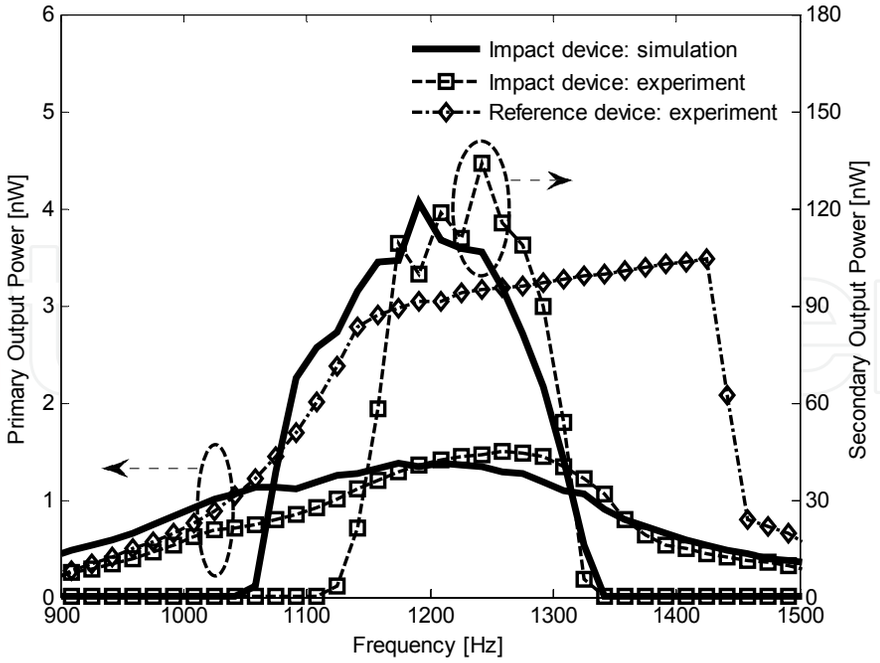

Figure 12. Output power frequency responses of the primary and secondary transducers in the impact device compared to the output from the reference device at RMS acceleration of 5.5g and bias voltage V_b=7V

Figure 13 compares the output powers of the reference and impact devices under bias voltage V_b=7V and at their resonance frequencies. For the impact device, the total output power is the sum of the primary and secondary output powers. For small accelerations, the primary mass does not impact on the secondary mass. The total output power is only contributed from the primary transducer. As a result, the total output power of the impact device is less than that of the reference device. For RMS accelerations larger than 3.5g, the primary mass begins to impact on the secondary structure. The secondary output voltage is dominant for RMS accelerations greater than 4.5g, giving a total output power significantly higher than that of the reference device. For example, the total output power of the impact device is approximately 200nW at an RMS acceleration of 5.5g, 33 times greater than RMS output power of the reference device which is 6.1nW. Further increase of the acceleration amplitude causes the secondary structure's motion to be limited by its own rigid end-stops. In this case, the impact device saturates at much higher output power level than the reference device does. Since the proof-mass displacement constraint is the same for both devices and the masses are about the same, this means that the secondary transducers have provided a dramatic increase in the harvester effectiveness.

Figure 14 illustrates the frequency response of the total output power of the impact device and the reference device in frequency up- and down sweeps at an acceleration amplitude of 5.5g and bias voltage V_b=7V. The total output power of the impact device is considerably higher than that of the reference device in the frequency range of secondary-transducer activation. There is no jump phenomenon or hysteresis in the frequency response of the impact device at such accelerations. This differs from the reference device.

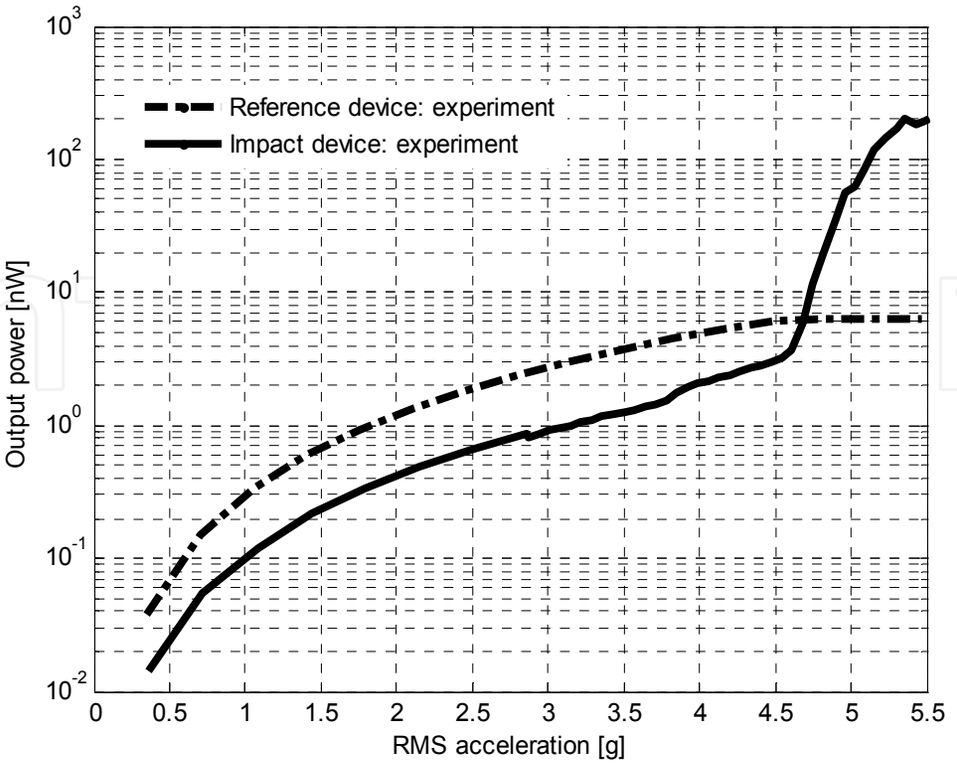

Figure 13. Comparison between measured output power of the reference and impact devices for bias voltage V_b=7V at resonance frequencies

One notable difference between this encapsulated low-Q device and the unpackaged high-Q device presented earlier [29] is the large difference in the RMS acceleration that is required for end-stop engagement. It is rather obvious that the difference in Q is responsible for this, but for both devices a subsequent additional increase in RMS acceleration is necessary before the output of the secondary transducers become appreciable, in the present device from 3.5g to 4.5g. For future designs, measures should be taken to ensure that the end-stop transducers are effective already when actuated a small distance so as to narrow down this range of RMS accelerations.

The merits of the impact-device concept can be quantified through the figure of merit *energy harvester effectiveness* as defined in [1]. Some example values are given for the present packaged device and a previous unpackaged device in Table 3. For conventional energy harvesters operating in the linear regime with displacement less than the limit X_{max}, the effectiveness is proportional to the acceleration amplitude. Then, it degrades as the acceleration amplitude increases beyond the value needed to reach the maximum amplitude X_{max}. This behaviour is displayed by the reference-device values in the table. With the active end-stops, the extra power improves the harvester effectiveness under displacement-limited operation. For the packaged devices presented in this book chapter, the effectiveness of the impact device is 4.25%, while this value is only of 0.11% for the reference device in the impact regime. The high mechanical quality factor Q in the previous unpackaged devices gives an even larger effectiveness up to 23.12%. Microscale energy harvesters have typical effectiveness in the range from 1% to 10% and it is lower

for smaller displacement limits [1]. The impact devices therefore achieve effectiveness values under displacement-limited operation that are comparable, or even favourable, in comparison with other device prototypes in [9, 15, 17-18, 33-36] with the same scale of the displacement limit. Together these examples show that there is much to be gained from transducing end-stops.

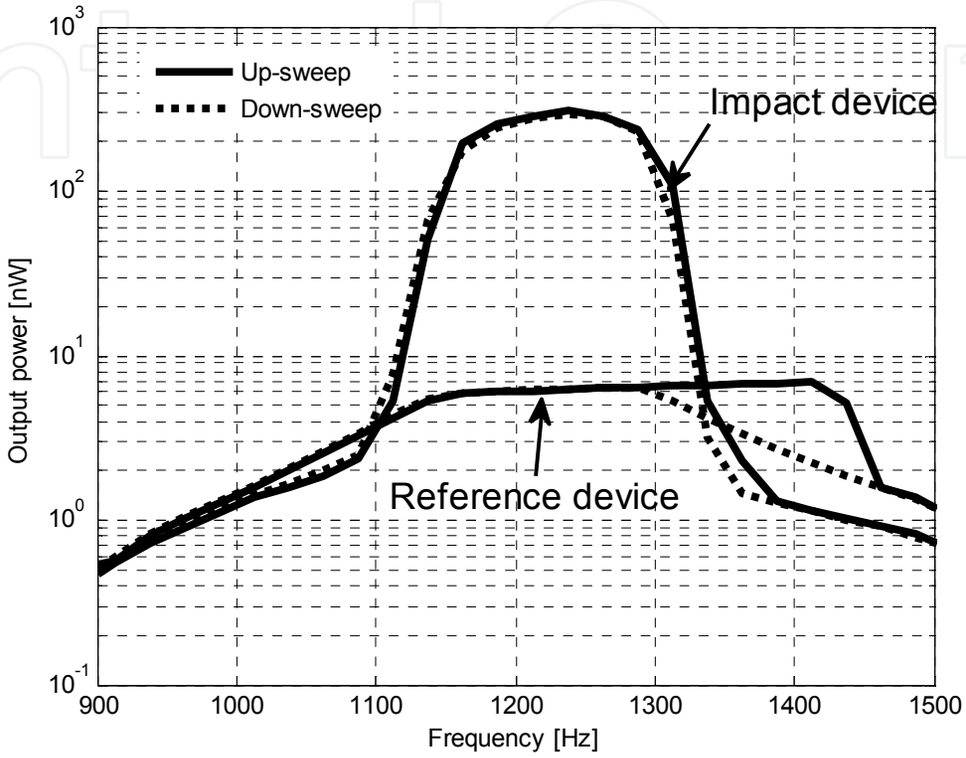

Figure 14. Frequency response of the measured output power of the reference and impact devices for a RMS acceleration of 5.5g and bias voltage V_b=7V

Packaged prototype, X_{max}=7μm				**Unpackaged prototype, X_{max}=10μm [29]**			
RMS acceleration amplitude [g]		**Effectiveness [%]**		**RMS acceleration amplitude [g]**		**Effectiveness [%]**	
		Reference device	**Impact device**			**Reference device**	**Impact device**
Linear regime	2.10	0.074	0.037	**Linear regime**	0.04	11.18	9.56
	4.19	0.145	0.078		0.06	17.42	14.81
Impact regime	5.15	0.139	3.017	**Impact regime**	1.76	5.40	14.44
	5.50	0.106	4.249		1.87	5.09	23.12

Table 3. Comparison of harvester effectiveness between the reference and impact devices

6. Conclusion

An electrostatic energy harvester with in-plane overlap-varying transducers on the primary mass and with secondary gap varying transducers as end-stops has been designed, modeled and characterized. The simulations are consistent with the measurement results. The performance was compared with that of a standard in-plane- overlap-varying type device. With the transducing end-stops we have seen that a considerable performance boost is obtained, with output power up to a factor 33 over the reference device, even though the reference device performed a factor of 3.4 better at low acceleration levels. None of the typical jump phenomena were observed in up and down frequency sweeps for this device. The frequency response of the impact device had approximately the same bandwidth as the reference device had on down sweeps.

Author details

Cuong Phu Le and Einar Halvorsen
Department of Micro and Nano Systems Technology,
Faculty of Technology and Maritime Sciences, Vestfold University College, Tønsberg, Norway

Acknowledgement

This work was financially supported by the Research Council of Norway under grant 191282. We thank Prof. Eric Yeatman and Prof. Oddvar Søråsen for useful discussions and suggestions.

7. References

[1] Mitcheson P D, Yeatman E M, Rao G K, Holmes A S, Green T C. Energy harvesting from human and machine motion for wireless electronic devices. Proceedings of the IEEE 2008;96(9) 1457-1486.
[2] Beeby S P, Tudor M J, White N M. Energy harvesting vibration sources for microsystems applications. Measurement Science and Technology 2006;17 175-195.
[3] Roundy S, Wright P K, Rabaey J. A study of low level vibrations as a power source for wireless sensor nodes. Computer Communications 2003;26 1131-1144.
[4] Roundy S, Steingart D, Frechette L, Wright P, Rabaey J. Power sources for wireless sensor networks. Computer Science 2004;2920:1-17.
[5] Starner T, Paradiso J A. Human generated power for mobile electronics. In: Piguet C. (ed.) Low-Power Electronics. Boca Raton FL: CRC Press; 2004. p1-35.
[6] Cantatore E, Ouwerkerk M. Energy scavenging and power management in networks of autonomous microsensors. Microelectronics Journal 2006; 37(12) 1584-1590.
[7] http://www.perpetuum.com/fsh.asp/ (accessed 19 June 2012).
[8] Anton S R, Sodano H A. A review of power harvesting using piezoelectric materials (2003–2006). Journal of Smart Materials and Structures 2007;16 1–21.

[9] Williams C B, Yates R B. Analysis of a micro-electric generator for microsystems. Sensors and Actuators A: Physical 1996;52 8-11.

[10] Mitcheson P D, Miao P , Stark B H, Yeatman E M, Holmes A S, Green T C. MEMS electrostatic micropower generator for low frequency operation. Sensors and Actuators A: Physical 2004;115 523–529.

[11] Naruse Y, Matsubara N, Mabuchi K, Izumi M, Suzuki S. Electrostatic micro power generator from low frequency vibration such as human motion. Journal of Micromechanics and Microengineering 2009;19 094002.

[12] Ferrari M, Ferrari V, Guizzetti M, Marioli D, Taroni A. Piezoelectric multifrequency energy converter for power harvesting in autonomous microsystems. Sensors and Actuators A: Physical 2008;142 329–335.

[13] Koukharenko E, Beeby S P, Tudor M J, White N M, O'Donnell T, Saha C, Kulkarni S, Roy S. Microelectromechanical systems vibration powered electromagnetic generator for wireless sensor applications. Journal of Microsystems Technology 2006;12(10) 1071–1077.

[14] Beeby S P, Torah R N, Tudor M J, Glynne-Jones P, O'Donnell T, Saha C, Roy S. A micro electromagnetic generator for vibration energy harvesting. Journal of Micromechanics and Microengineering 2007;17 1257–1265.

[15] Tvedt L, Blystad L-C J, Halvorsen E. Simulation of an electrostatic energy harvester at large amplitude narrow and wide band vibrations. In: Proceedings of Symposium on Design, Test, Integration, Packaging of MEMS/MOEMS, 9-11 April 2008, Nice, France; 2008.

[16] Soliman M S M, Abdel-Rahman E M, El-Saadany E F, Mansour R R. A wideband vibration-based energy harvester. Journal of Micromechanics and Microengineering 2008;18 115021.

[17] Hoffmann D, Folkmer B, Manoli Y. Fabrication, characterization and modeling of electrostatic micro-generators. Journal of Micromechanics and Microengineering 2009;19 094001.

[18] Blystad L-C J, Halvorsen E. A piezoelectric energy harvester with a mechanical end stop on one side. Journal of Microsystems Technology 2011;17 505-511.

[19] Blystad L-C J, Halvorsen E, Husa S. Piezoelectric MEMS energy harvesting driven by harmonic and random vibrations. IEEE Transactions on Ultrasonics, Ferroelectrics, and Frequency Control 2010;57(4) 908-919.

[20] Liu H, Tay C J, Quan C, Kobayashi T, Lee C. Piezoelectric MEMS energy harvester for low-frequency vibrations with wideband operation range and steadily increased output power. Journal of Microelectromechanical systems 2011;20(5) 1131-1142.

[21] Moss S, Barry A, Powlesland I, Galea S, Carman G P. A broadband vibro-impacting power harvester with symmetrical piezoelectric bimorph-stops. Journal of Smart Materials and Structures 2011;20 045013.

[22] Umeda M, Nakamura K, Ueha S. Energy storage characteristics of a piezo-generator using impact induced vibration. Japanese Journal of Applied Physics 1997, 36:3146–3151.

[23] Xu C-N, Akiyama M, Nonaka K, Watanabe T. Electrical power generation characteristics of PZT piezoelectric ceramics. IEEE Transactions on Ultrasonics, Ferroelectrics, and Frequency Control 1998;45 1065–1070.

[24] Funasaka T, Furuhata M, Hashimoto Y, Nakamura K. Piezoelectric generator using a LiNbO3 plate with an inverted domain. In: Proceeding of Symposium on IEEE Ultrasonics, 5–8 October, Sendai, Japan; 1998.

[25] Yoon S H, Lee Y H, Lee S W, Lee C. Energy-harvesting characteristics of PZT-5A under gunfire shock. Materials Letters 2008;62 3632-3635.

[26] Djugum R, Trivailo P, Graves K. A study of energy harvesting from piezoelectrics using impact forces. The European Physical Journal Applied Physics 2009;48(01) 11101.

[27] Gu L, Livermore C. Impact-driven, frequency up-converting coupled vibration energy harvesting device for low frequency operation. Journal of Smart Materials and Structures 2011;20 045004.

[28] Le C P, Halvorsen E, Søråsen O, Yeatman E M. An electrostatic energy harvester with power-extracting end stops driven by wideband vibrations. In: Proceedings of the PowerMEMS2011 Workshop, 5-18 November, Seoul, Korea; 2011.

[29] Le C P, Halvorsen E, Søråsen O, Yeatman E M. Microscale electrostatic energy harvester using internal impacts. Journal of Intelligent Material Systems and Structures 2012; DOI: 10.1177/1045389X12436739.

[30] Le C P, Halvorsen E. MEMS electrostatic energy harvesters with end-stop effects. Journal of Micromechanics and Microengineering 2012;22 074013.

[31] http://www.tronicsgroup.com/full-service-MEMS-foundry/ (accessed 19 June 2012).

[32] Kaur S, Halvorsen E, Søråsen O, Yeatman E M. Numerical analysis of nonlinearities due to rigid end-stops in energy harvesters. In: Proceedings of the PowerMEMS2010 Workshop, 30 Nov-3 December, Leuven, Belgium; 2010.

[33] Mizuno M, Chetwynd D G. Investigation of a resonance microgenerator. Journal of Micromechanics and Microengineering 2003;13 209–216.

[34] Miyazaki M, Tanaka H, Ono G, Nagano T, Ohkubo N, Kawahara T, Yano K. Electric-energy generation using variable-capacitive resonator for power-free LSI: efficiency analysis and fundamental experiment. In: Proceeding of the 2003 International Symposium on Low Power Electronics and Design, 25-27 August, Seoul, Korea; 2003.

[35] Despesse G, Chaillout J, Jager T, Leger J M, Vassilev A, Basrour S, Charlot B. High damping electrostatic system for vibration energy scavenging. In: Proceeding of the Joint Conference on Smart Objects and Ambient Intelligence, 12-14 October, Grenoble, France; 2005.

[36] Miao P, Mitcheson P D, Holmes A S, Yeatman E M, Green T C, Stark B H. MEMS inertial power generators for biomedical applications. Journal of Microsystem Technology 2006;12 1079–1083.

IntechOpen